Proceedings of IMECE'03
2003 ASME International Mechanical Engineering Congress
Washington, D.C., November 15–21, 2003

IMECE2003-41313

# DYNAMIC MODELING OF A THERMALLY-DRIVEN MICRO DIFFUSER PUMP

**Chen-li Sun**
Department of Mechanical Engineering
National Taiwan University of Science and Technology
Taipei, 106 Taiwan
clsun@mail.ntust.edu.tw

**Albert P. Pisano**
Berkeley Sensor and Actuator Center
University of California
Berkeley, CA 94720-1774, USA
appisano@me.berkeley.edu

## ABSTRACT

In this study, we present the dynamic modeling of a micro diffuser pump by employing the commercial software package CFDRC. Two types of time-dependent pressure boundary conditions are applied to the inlet. Sinusoidal and square wave functions with various amplitudes and frequencies are used. The results indicate a rectification effect such that a net flow in the divergent direction of the diffuser is gained over the time. In addition, the model is able to show the correlation of flow rate with frequency by flow circulation effects. This impact of the transient flow on the pumping performance is discussed. The modeling results are also compared to experimental data found in the literature. The net flow rates predicted by the 3D modeling are found to have good agreement at low excitation frequencies. To evaluate the validity of the imposed pressure boundary condition, the heat transfer model of the evaporation process is used.

Keywords: microfluidic, diffuser, micro pump, modeling, evaporation, MEMS

## INTRODUCTION

Micropumps have played a significant role in a wide variety of applications in microsystems including micro mixers , electronic cooling [1], μ-TAS (micro-total analysis systems) [2] and perhaps even micro internal combustion engines [3] and fuel cells [4]. Among different designs, there is considerable interest in the development of a nozzle-diffuser pump due to its simplicity and feasibility. An appropriately-designed diffuser has the fluid directing properties such that there is a lower flow resistance in the divergent direction than in the convergent direction. Based on this principle, a net flow in the divergent direction can be acquired by inciting an oscillating pressure gradient across the diffuser. In recent reports, researchers have used moving diaphragms [5, 6] or thermal bubbles [7] to actuate this necessary pressure oscillation.

The thermal bubble-actuated mechanism utilizes the expanding and collapsing actions of the bubbles to propel liquid. With the advantage of no moving parts, it not only reduces the risk of fatigue and wear, but also possibly simplifies the fabrication process. The pulsatile behavior of the bubble is controlled by the polysilicon heater and usually requires 5 to 10 W [8] of peak power input. However, this high power consumption is not acceptable for microscale power generation devices like the MEMS rotary engine power system [3] (REPS) or fuel cell power module. Since the goal of these devices is to output electrical power, the auxiliary requirements for electrical heating must be minimized. Therefore, the mechanism proposed here is to deliver vaporized fuel by recycling waste heat from the combustion/chemical process in the microsystems. By locating an evaporation zone downstream, the proposed design exploits the intermittent characteristics of the boiling process [9] to produce the required flow fluctuation in the diffuser. The schematic of this dynamic micro fuel evaporator is depicted in Fig. 1. In addition to the diffuser, the evaporation at the meniscus also helps to evoke a slow pumping effect [10] to the fluid.

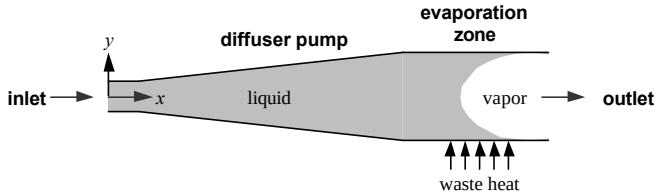


**Fig. 1 Schematic of the dynamic micro fuel evaporator**

In order to obtain the optimal design of the fuel evaporator for the MEMS REPS, understanding the dynamic characteristics of the micro diffuser pump is essential. Although several researches have modeled the diffuser pump, these

previous efforts were limited to steady flow conditions [11-13]. None has successfully analyzed the transient behavior that reflects the actual operation of the micro diffuser pump. Therefore, a numerical investigation is performed here to focus on the dynamic aspects. As a first step, two types of pulsatile pressures are applied as the boundary conditions: sinusoid and square wave. The numerical results for both wave types show that the net flow rate increases with the pressure amplitude but decreases with the excitation frequency. We also use a bubble growth model [14] to calculate the superheat variation corresponding to the pulsatile heating from the polysilicon heater. The pressure is then evaluated to discuss the validity of our hypothetical boundary conditions. The Reynolds number is relatively small (~500), validating the laminar flow assumption in the model.

## NOMENCLATURE

| | |
|---|---|
| $A$ | area, $m^2$ |
| $C_b$ | bubble growth rate constant |
| $C_p$ | thermal capacity, J/kg· K |
| $D$ | bubble diameter, m |
| $F$ | modification factor |
| $f$ | excitation frequency, Hz |
| $h$ | heat transfer coefficient, $W/m^2$· K |
| $h_{lv}$ | latent heat, J/kg |
| $k$ | thermal conductivity, W/m· K |
| $l$ | length, m |
| $P$ | pressure, kPa |
| $\dot{Q}$ | flow rate, µl/s |
| $R_0$ | reference electrical resistance, Ω |
| $T$ | temperature, K |
| $t$ | time, s |
| $\Delta t$ | time step, s |
| $V_{in}$ | input voltage, volts |
| $w$ | width, m |
| $y$ | thickness, m |

### Greek symbols

| | |
|---|---|
| $a$ | thermal diffusivity $a = \frac{k}{r \cdot C_p}$, $m^2/s$ |
| $c$ | rectification efficiency |
| $q$ | contact angle, rad |
| $r$ | density, $kg/m^3$ |
| $x$ | thermal coefficient of resistance, $K^{-1}$ |

### Miscellaneous subscript symbols

| | |
|---|---|
| $b$ | bubble |
| $evp$ | evaporation |
| $g$ | Petri dish |
| $l$ | liquid |
| max | maximum |
| $n$ | nitride |
| net | net |
| $p$ | polysilicon |
| $s$ | silicon |
| $sat$ | saturation |
| $v$ | vapor |

## MODEL CONSTRUCTION

*1. Simulation Domain*

In this investigation, we apply symmetric boundary conditions in the transverse and perpendicular directions. The simulation domains are chosen as a half of the diffuser for 2D, and a quarter for 3D modeling, as shown in Fig. 2, to minimize the memory requirement and computational time. The geometry of the simulation domain consists of the diffuser in the middle and two 300 µm long sections for inlet and outlet on both sides. The inlet of the diffuser is 30 µm wide, the length is 1987 µm, and the half angle is 7°. The height of the model is 25 µm for the 3D models.

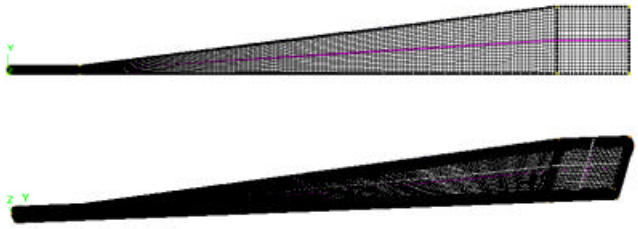

**Fig. 2 Simulation domains for 2D and 3D models with mesh**

*2. Feasibility Verification*

Since the previous works focused on higher ranges of flow rates (10 ~ 1000 µl/s) [5-7], we initially conduct a feasibility study for integration of the diffuser pump into the 2.4 mm MEMS REPS which requires a much lower flow rate. Velocity-driven flow is modeled to check the pressure variation at the inlet. The enforced velocity is based on the flow rate specification from the engine geometry, and then superposed with a sinusoidal oscillation to construct the boundary condition.

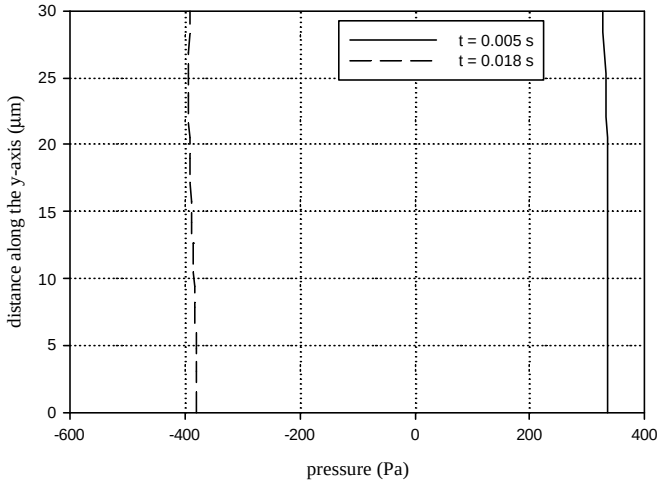


**Fig. 3 Pressure distributions at the inlet of the micro diffuser pump for velocity-driven flow, velocity amplitude = 0.3 m/s**

The frequency is set to 40 Hz, and three different velocity amplitudes are tested: 0.03, 0.3, and 1.0 m/s. When the velocity profile alters directions, the gauge pressures at the inlet indicate

sign changes accordingly for all three tested velocity amplitudes. The pressure distributions at the inlet are shown in Fig. 3 for $t$ = 0.005 s (positive velocity) and $t$ = 0.018 s (negative velocity). The maximum magnitude of the negative pressure is found to exceed that of the positive pressure for the velocity-driven flow. This means that it requires higher pressure to drive the flow in the convergent direction. Namely, the flow resistance in the divergent direction is lower, and the micro diffuser pump will indeed work in the operational flow rate range (~0.01 to 0.1 μl/s) against a pressure head of –400 Pa to 340 Pa.

*3. Sensitivity of Simulation Parameters*

The sensitivity analysis of the grid resolution is carried out by successively refining the mesh size and computing the corresponding net flow rate, as shown in Fig. 4. The net flow rate is evaluated by dividing the trapezoidal integration of the time-dependent flow rate over the total simulated time. It is found that the deviation of the net flow rate to the mesh size is within 13 %, and the average sensitivity of the mesh size is $1.4\times10^{-5}$ μl/s μm$^3$. Considering the computational time, simulations are performed at average mesh sizes of 56.4 μm$^2$ for 2D modeling, and 74.2 μm$^3$ for 3D modeling. From Fig. 4, the flow rate for the 56.4 μm$^2$ mesh shows a 8.6 % deviation from that of the finest mesh tested (12.1 μm$^2$).

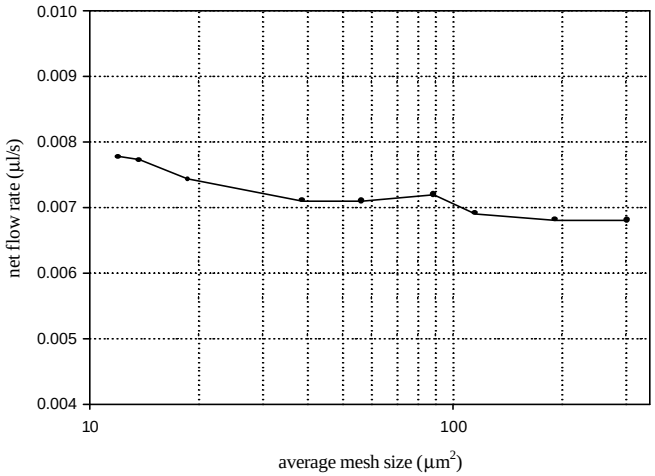


**Fig. 4 Mesh size dependence study for 2D model, sinusoidal pressure, P = 100 Pa, f = 40 Hz**

Different time steps and grid shapes (quadrangular/triagonal cells) were also tested, but their impacts on the net flow rate were negligible.

*4. Comparison of Transient and Steady State Results*

The steady state simulation with the same geometry is also performed for comparison. The pressure gradient is fixed at 100 Pa. The net flow rate evaluated by taking the difference of steady flow rates in two directions is 4.08 times larger than the result with a sinusoidal boundary condition ($P$ = 100 Pa, $f$ = 40 Hz). This demonstrates that the steady state assumption is not valid to reveal the dynamic operation of the micro diffuser pump; thus it is essential to use transient modeling for this type of problem.

## RESULTS

Simulations with oscillating pressures at the inlet boundary are accomplished with various amplitudes and frequencies. A typical volumetric flow rate is plotted in Fig. 5 for sinusoidal pressure, $P$ = 500 Pa and $f$ = 20 Hz. The corresponding pressure boundary condition is also shown in the figure for reference. From Fig. 5, it can be seen that the maximum magnitude of the flow rate in the divergent direction (forward) is almost twice as that in the convergent direction (backward). This indicates that a net flow is attainable with an oscillating pressure-driven flow, and CFDRC can be used to capture the rectification effects of micro diffuser pumps.

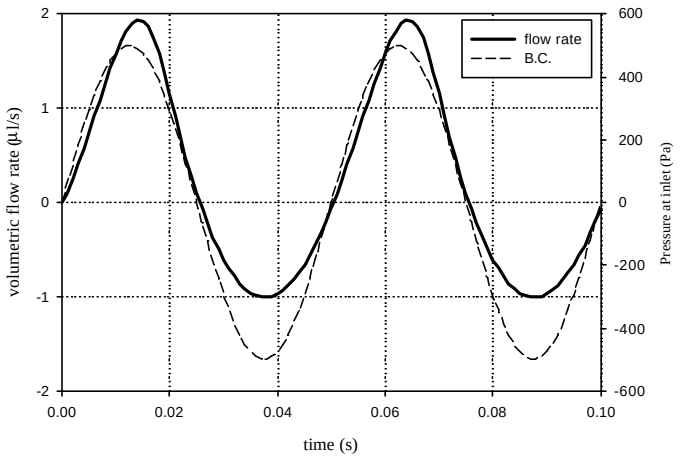


**Fig. 5 Volumetric flow rate vs. time with sinusoidal pressure at the inlet, P = 500 Pa, f = 20 Hz (2D model)**

The peak of the flow rate experiences a 1.5 ms delay in response to the varying pressure. This time delay is also observed at other amplitudes and frequencies, and is inferred from the slow flow development. Figure 6 (a) and (b) show the velocity profiles at the instants that the pressure gradients change from negative to positive and positive to negative, respectively. At those instants, the pressure gradients become unfavorable, i.e. pressure decreases in the flow direction [15]. From Fig. 6, the unfavorable pressure gradients cause flow circulations near the diffuser outlets. Although the circulations soon disappear after the flows become more developed, they result in the reduction of the attainable net flow rate.

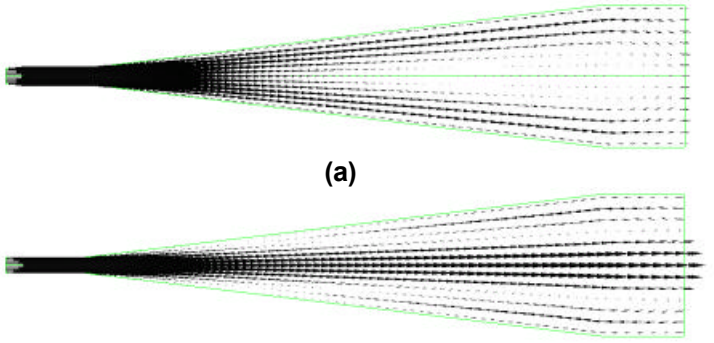

**(a)**

**(b)**

**Fig. 6 Velocity profile for sinusoidal pressure, P = 500 Pa, f = 20 Hz, (a) t = 0.051 s, (b) t = 0.075 s (2D model)**

From the transient results, the net flow rate is evaluated by the following steps. First, the instantaneous flow rates are collected for each time step. The net flow is then evaluated by trapezoidal integration of these instantaneous flow rates over the entire simulation time. Finally, we divide the net flow by the total time to obtain the net flow rate.

$$\dot{Q}_{net} = \frac{\sum_{i=0}^{n-1}\left[\frac{1}{2}\left(\dot{Q}_i + \dot{Q}_{i+1}\right)\cdot \Delta t\right]}{n \cdot \Delta t} \quad (1)$$

Since the simulation domains are a half and a quarter of the diffuser for the 2D and 3D models, respectively, the net flow rate is restored accordingly to reflect the symmetric assumptions.

The net flow rates for sinusoidal pressures with various amplitudes and oscillation frequencies are shown in Fig. 7. For $P$ = 500 Pa, the net flow rate deteriorates with the increase of the frequency. When the diffuser pump operates at lower frequencies, the rate of pressure change is slower and provides more time for the flow to be rectified. At higher frequencies, the circulation effect dominates and causes a reduction in the net flow rate. However, for $P$ = 100 Pa, the net flow rate is maintained around $7.5\times10^{-3}$ μl/s and is almost independent of the excitation frequency. Since the velocities are relatively small, the circulation effect is almost negligible for low-pressure amplitude.

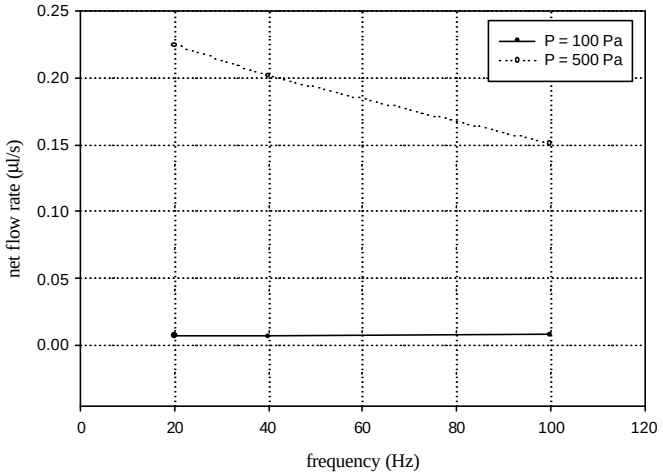


**Fig. 7 Net flow rate vs. frequency for sinusoidal pressure (2D model)**

Three-dimensional modeling is also conducted for the sinusoidal pressure boundary conditions. Since the channel depth is only 50 μm, it is necessary to examine the viscous effects from the top and bottom walls of the diffuser. The comparisons of the 2D and 3D results are shown in Table 1. It is found that the net flow rates from the 3D results are usually on the order of 100 times smaller than their 2D counterparts. This shows that the drag from the top and bottom walls significantly reduces the net flow rate. One way to diminish this effect is etching a deeper channel during the fabrication process of the micro diffuser pump.

| $P$ (Pa) | $f$ (Hz) | 2D, $\dot{Q}_{net}$ (μl/s) | 3D, $\dot{Q}_{net}$ (μl/s) |
|---|---|---|---|
| 100 | 40 | $7.10\times10^{-3}$ | $1.05\times10^{-4}$ |
| 500 | 40 | $2.01\times10^{-1}$ | $2.49\times10^{-3}$ |
| 500 | 100 | $1.51\times10^{-1}$ | $2.43\times10^{-3}$ |

**Table 1: Flow rate comparisons for 2D and 3D models with sinusoidal pressure boundary conditions**

Besides the sinusoidal pressure, square-wave pressure boundary conditions are also simulated with various amplitudes and frequencies. The duty cycle is fixed at 10 % in this study. The result with $P$ = 500 Pa and $f$ = 20 Hz is shown in Fig. 8 along with the corresponding boundary condition. Due to the sudden jump of the pressure, the flow rate grows very rapidly during the pulse length. Then the flow rate diminishes to less than $10^{-3}$ μl/s within 8.9 ms after reaching the maximum.

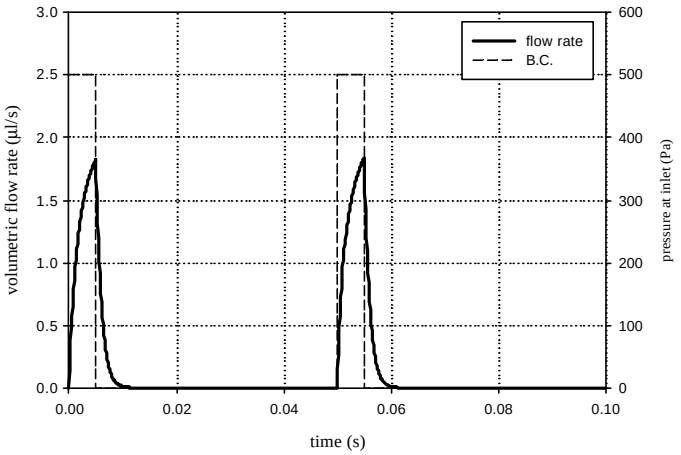


**Fig. 8 Volumetric flow rate vs. time with square-wave pressure at the inlet, P = 500 Pa, f = 20 Hz (2D model)**

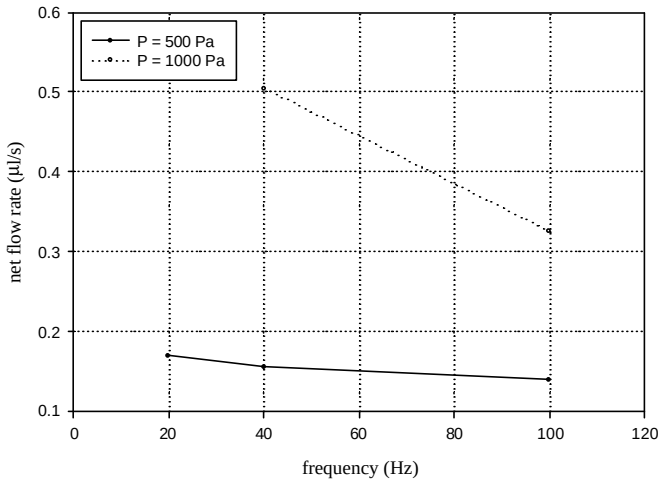


**Fig. 9 Net flow rate vs. frequency for square-wave pressure (2D model)**

For the square-wave pressure, flow circulations also appear near the outlet after the pulse (~ 5.6 ms). They persist throughout the rest of the cycle. The net flow rate for the

square-wave boundary conditions are plotted against frequency in Fig. 9. Characteristics similar to the sinusoidal condition are observed. The net flow rate is decreased with increasing frequency. Unlike the sinusoidal condition, the cause of this deterioration is more related to the decrease of the pulse length with frequency for a fixed duty cycle. According to Fig. 8, most of the net flow is gained during the pulse ($P > 0$). The longer the pulse length is, the higher the net flow rate can be achieved. This frequency dependence is particularly evident for high-pressure amplitude ($P = 1000$ Pa).

To indicate the pumping efficiency of the dynamic diffuser, the rectification efficiency, $c$, is defined as the net flow rate divided by the maximum forward flow rate:

$$c = \frac{\dot{Q}_{net}}{\dot{Q}_{\max}} \tag{2}$$

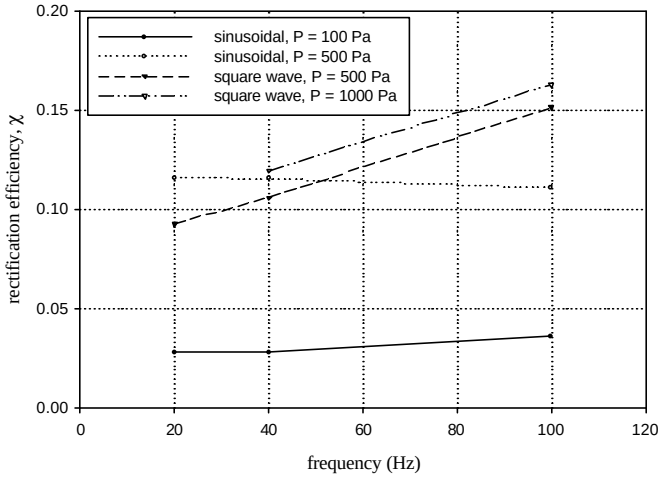


**Fig. 10 Rectification efficiency vs. frequency for 2D models**

The rectification efficiencies are shown in Fig. 10 for 2D models with sinusoidal and square-wave boundary conditions. With the sinusoidal pressure boundary conditions, $c$ is found to be nearly independent of frequency. The rectification efficiencies for $P = 500$ Pa are approximately 3 ~ 4 times larger than those for $P = 100$ Pa. The rectification efficiencies for 3D models under the same boundary conditions are much lower (< 0.01). Nevertheless, the rectification efficiencies show a stronger dependence on frequency for the square-wave boundary conditions. The values of $c$ decrease with increasing of frequency. This is because at higher frequency, the shorter pulse length results in a smaller maximum forward flow rate. In addition, the rectification efficiencies for $P = 1000$ Pa are approximately 10 % more than those for $P = 500$ Pa at the same frequencies.

## DISCUSSION

The CFD model is compared to experimental data from the literature [7], as shown in Fig. 11. The flow rate predicted by the 2D model overestimates the net flow rate because it does not consider the viscous effects from the top and bottom walls. On the other hand, the 3D models with $P = 500$ Pa show a good agreement with the experimental results at low frequencies.

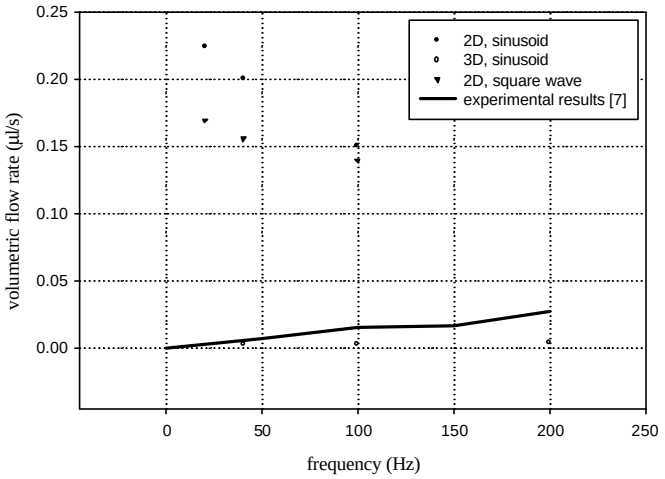


**Fig. 11 Volumetric flow rate comparison**

For the thermal bubble actuated nozzle-diffuser pump, the pressure head was reported to be around 100 Pa [7]. However, our 3D model was found to underestimate their experimental result for $P = 100$ Pa. Since the static pressure head does not reflect the dynamic pressure gradient across the micro diffuser in operation, a more detailed investigation is done to check the validity of the two tested boundary conditions. To serve this purpose, the model of bubble formation on a polysilicon heater [14] is introduced to estimate the pressure variation.

For the silicon substrate,

$$r_s C_{p,s} \frac{\partial T_s}{\partial t} = \frac{w_p \cdot l_p \cdot k_n}{w_s \cdot l_s \cdot y_s} \frac{(T_p - T_s)}{F \cdot y_n} - \frac{k_l}{y_s} \frac{(T_s - T_l)}{\sqrt{p a_l t}} - \frac{k_g (T_s - T_l)}{y_s \cdot y_g} \cdot \left[ 1 + 2\exp\left( -\frac{p^2 a_g t}{y_g^2} \right) \right] \tag{3}$$

For the polysilicon heater,

$$r_p C_{p,p} \frac{\partial T_p}{\partial t} = -\frac{k_n}{y_p} \frac{(T_p - T_s)}{F \cdot y_n} - \frac{(A_p - A_b) \cdot h_p (T_p - T_l) + A_b \cdot h_{evp} (T_p - T_{sat})}{w_p \cdot l_p \cdot y_p} + \frac{V_{in}^2}{w_p \cdot l_p \cdot y_p \cdot R_0 \left[ 1 + x (T_p - T_0) \right]} \tag{4}$$

where

$$A_p = l_p \cdot (w_p + 2y_p)$$

$$A_b = D \sin q \, (w_p + 2y_p)$$

$$h_p = h_{\max} \left[ 1 - \exp\left( -\frac{t}{t} \right) \right]$$

$$h_{evp} = r_v \cdot h_{lv} \frac{C_b}{\sqrt{t}} + k_l \frac{T_{sat} - T_l}{\sqrt{a_l t}} \frac{p \cdot C_b \sqrt{t} (1 + \cos q)}{(w + 2y_p) \sin (T_p - T_{sat})}$$

For a square-wave voltage input, the bubble grows when $V_{in} > 0$, and the bubble collapses when $V_{in} = 0$. From Eq. (3) and (4), $T_p$ and $T_s$ can be solved numerically, and they are shown in Fig. 11 for a square-wave voltage input with $V_0 = 20$

V, $f$ = 20 Hz, and duty cycle = 10 %. Since the time constant of the polysilicon heater is on the order of 0.1 μs, the surface temperature soars very rapidly and remains around 309 °C during the heating process. After the pulse, it quickly drops back to the ambient temperature. From Fig. 12, the polysilicon temperature variation is almost synchronic to the electrical power input. On the other hand, the time constant of the silicon substrate is on the order of 1 s. With a 5ms pulse length, the change of the silicon temperature is negligible and remains nearly constant throughout the simulation time.

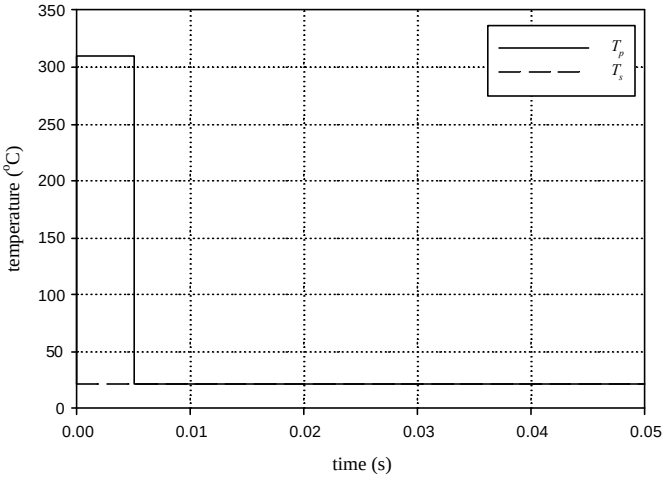


**Fig. 12 Temperature responses of polysilicon heater and silicon substrate for a square-wave voltage input, $V_0$ = 20 V, f = 20 Hz, duty cycle = 10 %**

Assuming the vapor inside the bubble is at the same temperature as the polysilicon, the vapor pressure can be calculated by the Clausius-Clapeyron equation:

$$P_v - P_l = \frac{r_v h_{lv} (T_v - T_{sat})}{T_{sat}} \quad (5)$$

From Eq. (5), $P_v - P_l$ is approximately 599 kPa for water. Due to the dissipation loss in the fluid, the actual pressure gradient across the diffuser should be much smaller than the value estimated by Eq. (5). By using the measurement of the acoustic pressure wave, peak pressure was reported to be about 20 kPa for a 6 μs pulse heating [16]. The aforementioned pressures suggest that larger pressure amplitudes should be used in the simulation.

The polysilicon heater usually generates explosive vaporization and provides more elevated peak pressures to the system. Therefore, the square-wave pressure boundary condition will probably depict the real operation of the diffuser pump better for the thermal bubble actuated mechanism. For the intermittent meniscus actuated mechanism, as schematically shown in Fig. 1, there is no embedded electrical heater. The sinusoidal pressure might be more appropriate for this geometry to represent the instability of the meniscus because it has a more gradual variation.

## CONCLUSIONS

The kinematic modeling of the micro diffuser pump is performed here for the first time. The rectification effects of the micro diffuser pump are demonstrated within the operational flow rate of the MEMS REPS. Two types of pressure boundary conditions are tested, sinusoidal and square wave. The maximum net flow rate predicted from the simulation is 0.504 μl/s for the square-wave pressure with $P$ = 1000 Pa and $f$ = 40 Hz. The maximum rectification efficiency, 0.163, is achieved for the square-wave pressure boundary condition with $P$ = 1000 Pa and $f$ = 100 Hz.

Despite the viscosity of water, the net flow rates from 3D model are found to be generally lower compared to experimental results. This suggests that the flow circulation might be numerically overestimated, especially at higher excitation frequencies. The difference of pressure boundary condition in simulations and the actual pressure variation caused by the fluctuating bubble might also contribute to the mismatch at higher frequency. Nevertheless, the 3D models with the sinusoidal pressure boundary conditions still show a satisfactory agreement with experimental results.

## ACKNOWLEDGMENT

This work is supported by DARPA under grant No. NBCHC010060. The authors would also like to express their gratitude to Prof. Dorian Liepmann and Mr. Luke Hunter of the University of California at Berkeley for their assistances with CFDRC.

## REFERENCES

[1] Jiang, L., Koo, J.-M., Zeng, S., Mikkelsen, J. C., Zhang, L., Zhou, P., Santiago, J. G., Kenny, T. W., Goodson, K. E., Maveety, J. G., and Tran, Q. A., 2001, "Two-Phase Microchannel Heat Sinks for an Electrokinetic Vlsi Chip Cooling System," Proceedings of the Proceedings of the Seventeenth Annual IEEE Semiconductor Thermal Measurement and Management Symposium (Cat. No.01CH37189), IEEE International, San Jose, CA, USA, pp. 153-157.

[2] Schluter, M., Kampmeyer, U., Tahhan, I., and Lilienhof, H. J., 2002, "A Modular Structured, Planar Micro Pump with No Moving Part (NMP) Valve for Fluid Handling in Microanalysis Systems," Proceedings of the Proceedings of the 2nd Annual International IEEE-EMBS Special Topic Conference on Microtechnologies in Medicine and Biology (Cat. No.02EX578), A. Dittmar, D. Beebe, eds., IEEE International, Madison, WI, USA, pp. 500-503.

[3] Fu, K., Knobloch, A. J., Martinez, F. C., Walther, D. C., Fernandez-Pello, A. C., Pisano, A. P., and Liepmann, D., 2001, "Design & Fabrication of a Silicon-Based MEMS Rotary Engine," Proceedings of the ASME 2001 International Mechanical Engineering Congress and R&D Expo, New York.

[4] Arana, L. R., Schaevitz, S. B., Franz, A. J., Jensen, K. F., and Schmidt, M. A., 2002, "A Microfabricated Suspended-Tube Chemical Reactor for Fuel Processing," Proceedings of the Technical Digest of MEMS 2002. Fifteenth IEEE International Conference on Micro Electro Mechanical Systems (Cat. No.02CH37266), IEEE International, Las Vegas, NV, USA, pp. 232-235.

[5] Olsson, A., Enoksson, P., Stemme, G., and Stemme, E., 1997, "Micromachined Flat-Walled Valveless Diffuser Pumps," Journal of Microelectromechanical Systems **6**(2), pp. 161-166.

 

[6] Olsson, A., Stemme, G., and Stemme, E., 1995, "A Valve-Less Planar Fluid Pump with Two Pump Chambers," Sensors & Actuators A-Physical **A47**(1-3), pp. 549-556.
[7] Tsai, J.-H. and Lin, L., 2002, "A Thermal-Bubble-Actuated Micronozzle-Diffuser Pump," Journal of Microelectromechanical Systems **11**(6), pp. 665-671.
[8] Tsai, J.-H., 2001, "Thermal Bubble Actuated Nozzle-Diffuser Micro Pump," Ph.D. Dissertation, University of Michigan, Ann Arbor, MI.
[9] Zhang, L., Koo, J.-M., Jiang, L., Goodson, K. E., Santiago, J. G., and Kenny, T. W., 2001, "Study of Boiling Regimes and Transient Signal Measurements in Microchannels," Proceedings of the Transducers '01/EUROSENSORS XV. Proceedings of 11th International Conference on Solid-State Sensors and Actuators, E. Obermeier, eds., Springer-Verlag, Munich, Germany, **2**, pp. 1514-1517.
[10] Namasivayam, V., Handique, K., Burke, D. T., Larson, R. G., and Burns, M. A., 2000, "Microfabricated Valveless Pump for Delivering Nonpulsatile Flow," Proceedings of the Proceedings of SPIE - Microfluidic Devices and Systems III, SPIE, Santa Clara, CA, USA, **4177**, pp. 220-228.
[11] Olsson, A., Stemme, G., and Stemme, E., 1997, "Simulation Studies of Diffuser and Nozzle Elements for Valve-Less Micropumps," Proceedings of the Tranducers '97. 1997 International Conference on Solid-State Sensors and Actuators. Digest of Technical Papers (Cat. No.97TH8267), IEEE, Chicago, IL, USA, **2**, pp. 1039-1042.
[12] Jiang, X. N., Zhou, Z. Y., Yang, Y., Huang, X. Y., and Liu, C. Y., 1997, "Experiments and Analysis for Micro-Nozzle/Diffuser Flow and Micro Valveless Pumps," Proceedings of the Tranducers '97. 1997 International Conference on Solid-State Sensors and Actuators. Digest of Technical Papers (Cat. No.97TH8267), IEEE International, Chicago, IL, USA, **1**, pp. 369-372.
[13] Olsson, A., Stemme, G., and Stemme, E., 2000, "Numerical and Experimental Studies of Flat-Walled Diffuser Elements for Valve-Less Micropumps," Sensors & Actuators A-Physical **A84**(1-2), pp. 165-175.
[14] Tsai, J.-H. and Lin, L., 2002, "Transient Thermal Bubble Formation on Polysilicon Micro-Resisters," Journal of Heat Transfer **124**(2), pp. 375-382.
[15] White, F. M., 1991, *Viscous Fluid Flow*, McGraw-Hill, New York.
[16] Zhao, Z., Glod, S., and Poulikakos, D., 2000, "Pressure and Power Generation During Explosive Vaporization on a Thin-Film Microheater," International Journal of Heat & Mass Transfer **43**(2), pp. 281-296.